

Evaluation of a large-eddy model simulation of a mixed-phase altocumulus cloud using microwave radiometer, lidar and Doppler radar data

By J. H. MARSHAM^{1*}, S. DOBBIE¹, R. J. HOGAN²

¹*University of Leeds, UK*

²*University of Reading, UK*

(Received 1 January 2000; revised 31 January 2001)

SUMMARY

Using the Met Office large eddy model (LEM) we simulate a mixed-phase altocumulus cloud, which was observed at Chilbolton in southern England by a 94 GHz Doppler radar, a 905 nm lidar, a dual wavelength microwave radiometer and also by four radiosondes. It is important to test and evaluate such simulations with observations, since there are significant differences between results from different cloud resolving models for ice clouds. Simulating the Doppler radar and lidar data within the LEM allows us to directly compare observed and modelled quantities and allows us to explore the relationships between observed and unobserved variables. For general circulation models, which currently tend to give poor representations of mixed-phase clouds, the case shows the importance of using: (i) separate prognostic ice and liquid water (ii) a vertical resolution that captures the thin layers of liquid water and (iii) accurately representing the sub-grid vertical velocities that allow liquid water to form.

It is shown that large scale ascents and descents are significant for this case and the horizontally averaged LEM profiles are relaxed towards observed profiles to account for these. The LEM simulation then gives a reasonable cloud, with an ice water path approximately two thirds of that observed, with liquid water at the cloud-top as observed. However, the liquid water cells that form in the updraughts at cloud-top in the LEM have a liquid water paths (LWPs) up to half those observed, and there are too few cells, giving a mean LWP five to ten times smaller than observed. In reality ice nucleation and fallout may deplete ice-nuclei concentrations at the cloud-top, allowing more liquid water to form there, but this process is not represented in the model. Decreasing the heterogeneous nucleation rate in the LEM increased the LWP, which supports this hypothesis. The LEM captures the increase in standard deviation in Doppler velocities (and so vertical winds) with height, but values are 1.5 to 4 times smaller than observed (although values are larger in an unforced model run this only increases the modelled LWP by a factor of approximately two). The LEM data show that, for values larger than approximately 12 cm/s, the standard deviation in Doppler velocities provide an almost unbiased estimate of the standard deviation in vertical winds, but provide an over-estimate for smaller values. Time-smoothing the observed Doppler velocities and modelled mass-squared-weighted fallspeeds shows that observed fallspeeds are approximately two-thirds of the modelled values. Decreasing the modelled fallspeeds to those observed increases the modelled IWC, giving an IWP 1.6 times that observed.

KEYWORDS: cloud radar cloud-resolving model ice nuclei

1. INTRODUCTION

Altocumulus and altostratus clouds cover approximately 22% of the Earth's surface (Warren et al., 1986, 1988) and play an important role in the climate system (Li and Le Treut, 1992; Sun and Shine, 1995). Mixed-phase layer clouds are, however, often poorly represented in numerical weather prediction models (Hogan et al., 2003b; Vaillancourt et al., 2003; Tremblay and Glazer, 2000; Tremblay et al., 2003). Cloud-resolving model (CRM) simulations of such clouds should allow us to understand the processes that must be included to model these clouds in GCMs and so lead to improved GCM parametrisations. Despite this, there are remarkably few published cloud-resolving model (CRM) simulations of mixed-phase altocumulus or altostratus clouds using high spatial resolutions (*i.e.* horizontal grid-spacings less than 1 km). Clark et al. (2005) explored the sensitivity of the LEM to changes in microphysics for a frontal mixed-phase cloud;

* Corresponding author: Institute for Atmospheric Science, School of the Earth and Environment, University of Leeds, Leeds, LS2 9JT, UK. Email: jmarsham@env.leeds.ac.uk

© Royal Meteorological Society, 2002.

Starr and Cox (1985) and Liu and Krueger (1995, 1998) all simulate similar liquid phase altostratus or altocumulus clouds; and Cotton and Brown (2004) applied their prognostic ice-nuclei scheme to an idealised mixed-phase altostratus cloud. Of these simulations only Clark *et al.* (2005) is directly compared with observations. Starr *et al.* (2000) showed a considerable variation between CRMs for cirrus clouds and we might expect a similar variation for stratiform mixed-phase clouds. As a result it is currently important to evaluate CRMs by comparing their results with observations.

In this paper we simulate a case of mixed-phase altocumulus observed by the 94 GHz radar and 905 nm lidar at Chilbolton in southern England using the Met Office large eddy model (LEM). To evaluate the ability of the LEM to represent a mixed-phase cloud we compare fields of observed and modelled variables. For the lidar and Doppler radar data this requires us to simulate the data within the LEM to account for the temporal and spatial sampling of the instruments. This then allows relationships between observed parameters (such as Doppler velocities) and unobserved parameters (such as fallspeeds and air velocities) to be explored, giving a better understanding of the observed quantities.

There have been several recent observational studies of mixed-phase layer clouds (Heymsfield *et al.*, 1991; Fleishauer *et al.*, 2002; Korolev and Isaac, 2003; Hogan *et al.*, 2003a,b; Field *et al.*, 2004; Hogan *et al.*, 2004) which have utilised both ground-based lidar and radar as well as aircraft data. *In-situ* measurements are invaluable for validating CRMs, but cloud observing radars and lidars are a very important source of data, since they are capable of continuously retrieving profiles of cloud parameters. Thus, they produce two-dimensional (space-time) fields, with similar spatial and temporal resolution to CRMs. In particular, whilst the radar can be used to retrieve ice water content (IWC) and fallspeeds, the lidar data indicate the position of any liquid water layers (which tend to be very reflective because of the small size and high number concentration of the supercooled water droplets compared with the ice particles). One limitation of such radars and lidars are their fixed location, but CloudSat and Calipso will soon give an unprecedented volume and spatial coverage from space (Stephens *et al.*, 2002).

Fallspeeds of ice crystals remain a significant uncertainty, which contributes to the spread in results from different models for clouds containing ice (Starr *et al.*, 2000). The radiative balance of global models has also been shown to be very sensitive to the specification of fallspeeds (Heymsfield and Iaquinta, 2000). Time-averaging of Doppler radar data is one method that has been used to retrieve fallspeeds (e.g. Matrosov *et al.* (1994), or Matrosov and Heymsfield (2000)) and in this paper this technique is applied to both real and simulated data and so used to evaluate the fallspeeds in the model.

Section 2 briefly describes the quantities retrieved from the 94 GHz radar and the 905 nm lidar at Chilbolton, UK. Section 3 describes the altocumulus case studied in this paper. Section 4 describes the LEM, including the model initialisation and the simulation of the observational data within model. Section 5 compares the real and simulated data as well as exploring the relationships between the quantities observed by the radar and the model variables. This allows us to test not only the LWC and IWC, but also the vertical winds and fallspeeds simulated by the LEM. The importance of the liquid water content (LWC) to the radiative processes in the cloud is examined in Section 5(e).

2. DATA FROM THE CHILBOLTON 94 GHz DOPPLER RADAR AND 905 NM LIDAR

(a) *The Chilbolton 94 GHz Doppler radar*

The 94 GHz radar at Chilbolton has been in near continuous operation since 1996 and Doppler data has been available since 2001. The radar emits 6250 pulses per second, each equivalent to around 60 m in length, and at 7 km, about 70 m wide. The pulses are averaged in real-time to get 1.25 s resolution. Every thirty seconds the following parameters are calculated from these 1.25 s data:

1. Mean radar reflectivity factor, Z . This (in combination with temperatures from a forecast model) is then used to estimate the mean IWC (Hogan et al., 2006).
2. The mean Doppler velocity, V_D , using only the data where a detectable signal was returned.
3. The standard deviation in the Doppler velocities, $\sigma(V_D)$, only if a detectable signal was present for all twenty four 1.25 s intervals. This parameter provides information on turbulence (Bouniol et al., 2003).
4. The mean spectral width of the Doppler velocities, using only the data where a detectable signal was returned. This parameter can be difficult to interpret, because it contains information from both turbulence and the spread of terminal fallspeeds, so is not used in this paper (although simulating this parameter may allow a better understanding of its significance, as discussed in Section 5(c)).

In ice clouds the measured Doppler velocity is a function of the vertical velocities of the ice particles in the radar beam and so depends on both the terminal fallspeeds of the ice and also the vertical velocity of the air. The radar backscatter is more sensitive to the larger particles (in the Rayleigh scattering regime it is sensitive to the radius to the power six, or the mass squared), so the Doppler velocity retrieved, V_D , is the sum of the vertical air velocity, w , and the mass-squared-weighted fallspeed, V_Z :

$$V_D = w - V_Z = w - \frac{\int_0^\infty n(M)V(M)M^2dM}{\int_0^\infty n(M)M^2dM}. \quad (1)$$

$V(M)$ is the terminal fallspeed of an ice particle of mass M and $n(M)dM$ is the number concentration of ice particles with mass between M and $M + dM$. At 94 GHz, Rayleigh scattering is a reasonable approximation if there are not a significant number of particles with diameters larger than $\simeq 1$ mm, which is supported by the radar data and the LEM in this case. The radar return can still be used to retrieve the IWC when liquid water is present, because the radar return is dominated by the ice particles, which are much larger than the liquid water droplets.

(b) *The Chilbolton 905 nm lidar*

The attenuated backscatter coefficient, β' is recorded by the Vaisala 905 nm lidar ceilometer at Chilbolton, averaged over 30 s intervals, with a 30 m vertical resolution. In the absence of multiple scattering β' is given by,

$$\beta' = \beta \exp[-2\tau], \quad (2)$$

where β is the unattenuated backscatter coefficient and τ is the optical depth between the instrument and the height of observation, z .

$$\tau = \int_0^z \alpha dz, \quad (3)$$

where α is the extinction coefficient. Lidar is sensitive to small particles, particularly liquid water droplets, and is therefore complementary to the radar, which is dominated by larger ice particles (Hogan *et al.*, 2003a). However, a thin layer of liquid water (or a deep layer of ice) can attenuate the lidar beam, resulting in an unmeasurably small backscatter from any cloud above that level.

3. THE CASE-STUDY

A case of gradually deepening cloud, which was observed ahead of a cold front on the 5th of September 2003, was chosen because the number of radiosonde profiles available made it relatively straightforward to initialise the LEM (Section 4(a)). Figure 1(a) shows deepening inhomogeneous ice cloud over the radar from 05:00 UTC to 12:00 UTC. A comparison of the lidar (Figure 2) and radar data shows that the ice was falling from a layer of liquid water at the cloud top ($\simeq -20^\circ\text{C}$ at 6 km); the first published explanation of such layers, where updraughts allow the condensate supply rate to exceed the ice crystal growth rate, was given by Rauber and Tokay (1991). We expect that the large values of $\sigma(V_D)$ near cloud top (Figure 1(b) and also Figure 4(b) and (d)) were caused by radiative cooling to space (Section 5(e) shows that radiative cooling of the liquid water contributes significantly to this process). The larger vertical velocities near the cloud-top, where the largest values of $\sigma(V_D)$ are observed, allow air parcels to become saturated with respect to water as well as ice and so liquid water to form (as discussed by Rauber and Tokay (1991)). The lidar (Figure 2) shows that liquid water was also intermittently present near cloud base ($\simeq -13^\circ\text{C}$ at 5 km). This liquid water may form in updraughts in turbulence caused by the evaporation of falling ice. The lidar sensitivity is reduced by the sky background during the day, which explains its failure to detect the ice. The mean Doppler velocities decrease in magnitude with height (Figure 1(c)), because larger ice particles are present lower down in the cloud.

Four radiosondes (Figure 3) were launched from Larkhill (20 km from Chilbolton) at 05:00, 08:00, 10:00 and 12:00 UTC. These show the gradually deepening moist cloudy layer and a thin layer near cloud-top ($\simeq 450$ hPa), that is saturated with respect to liquid water. The cloud was also observed by ground-based dual-wavelength microwave radiometer at Chilbolton. This allowed the liquid water path (LWP) to be retrieved (e.g. Westwater (1978)).

Data from four numerical weather prediction (NWP) models were obtained from the EU CloudNet project. Interestingly, none of these models predicted this altocumulus case accurately. The European Centre for Medium-Range Weather Forecasts (ECMWF) model (12 to 35 hour forecasts) produced cloud in the right place, but the cloud was all an liquid/ice mixture with too much liquid. The fraction of ice in the ice/liquid mixture is diagnosed from temperature in the ECMWF model (Matveev, 1984) and so this scheme cannot be expected to represent the position of the thin liquid water layers. The Met Office mesoscale model (6 to 11 hour forecast) uses separate prognostic ice and water (Wilson and Ballard, 1999), but produced far less cloud than observed and no liquid. Météo

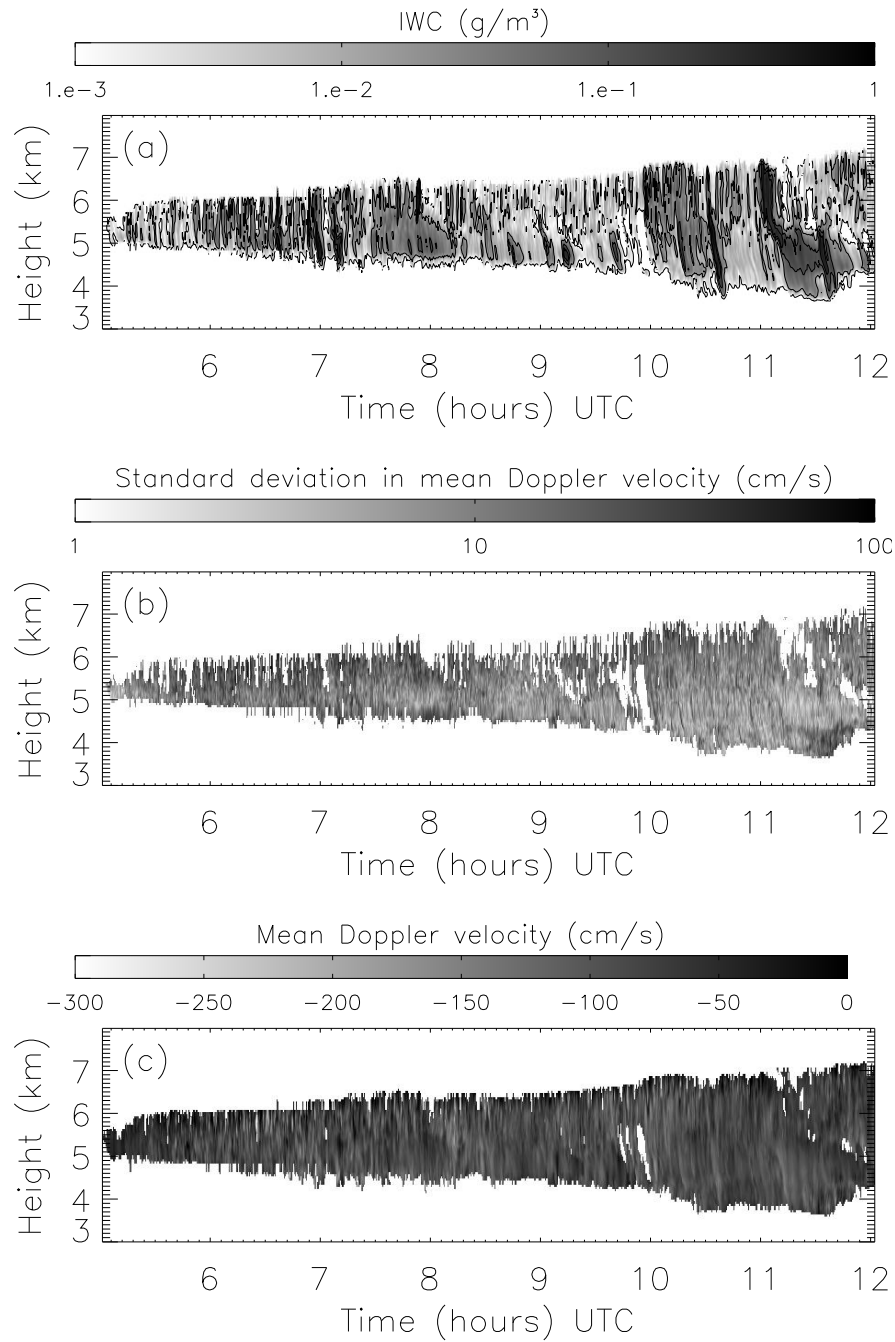


Figure 1. Observations from the Chilbolton 94 GHz radar on the 5th September, 2003. (a) IWC from the method of Hogan et al. (2006). Contours are at 0.001, 0.01 0.05 and 0.1 g/m^3 (b) The standard deviation in mean Doppler velocities, $\sigma(V_D)$ (c) The mean Doppler velocities, V_D .

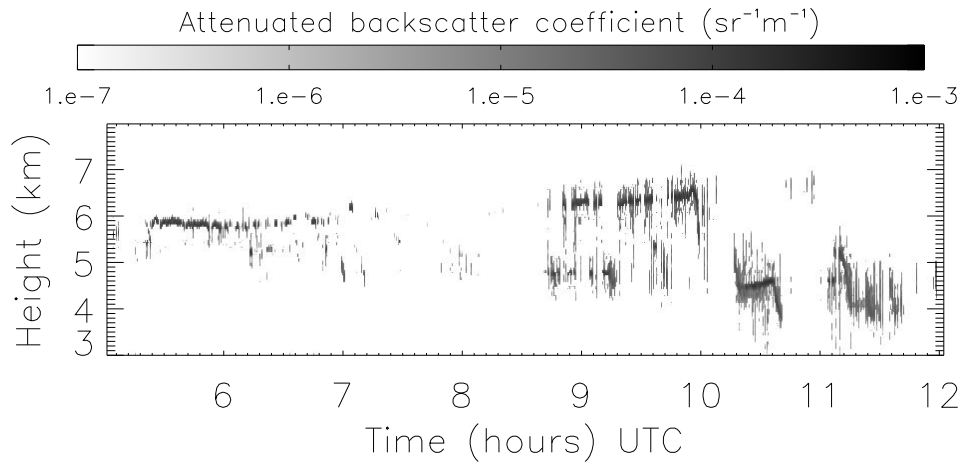


Figure 2. Observations from Chilbolton 905 nm lidar; liquid water at the cloud-top and near the cloud-base gives a strong backscatter. Daylight leads to reduced sensitivity and so the ice cannot be seen.

France (12 to 35 hour forecasts) predicted no cloud at all (the humidity was far too low). The Swedish Meteorological and Hydrological Institute (SMHI) Rossby Centre Regional Atmosphere (RCA) model, which is not SMHI’s operational model, also gave a poor representation with an incorrect humidity. These errors are not all from the simple representations of mixed-phase clouds used in these models, but also from synoptic or mesoscale errors in forecasts of parameters such as humidity. However, since the resolutions of these models are improving and the microphysical schemes are gradually becoming more sophisticated it is important to investigate to what extent a cloud resolving model, such as the Met Office LEM, can capture the cloud processes involved in this case. If the LEM represents these processes well it provides a useful tool for developing parameterisations for larger scale models.

4. METHOD

The case was simulated using an established cloud-model, the Met Office large eddy model (LEM). In order to evaluate the modelled cloud Doppler radar and lidar data were simulated (Section 4(b)). The model solves an anelastic quasi-Boussinesq set (Gray et al., 2001) and has a fully-integrated radiation model (Fu and Liou, 1992, 1993), although the effective radius of water and ice were fixed to $4.18 \mu\text{m}$ and $35 \mu\text{m}$ respectively in the radiative code, rather than being derived from the LEM fields. The radiation model is four-stream with six solar and twelve infrared bands and uses the independent column approximation. Ice is treated optically assuming hexagonal shapes (Fu, 1996; Fu et al., 1998) and a time-varying solar zenith angle was used. Double moment ice and snow† (*i.e.* prognostic mass and number) were used as well as prognostic water vapour and liquid water. The model was run in two dimensions, which is not unusual for CRM studies (e.g. Starr et al. (2000); Xu et al. (2002)). It would be straightforward

† Aggregated ice is called “snow” in the LEM.

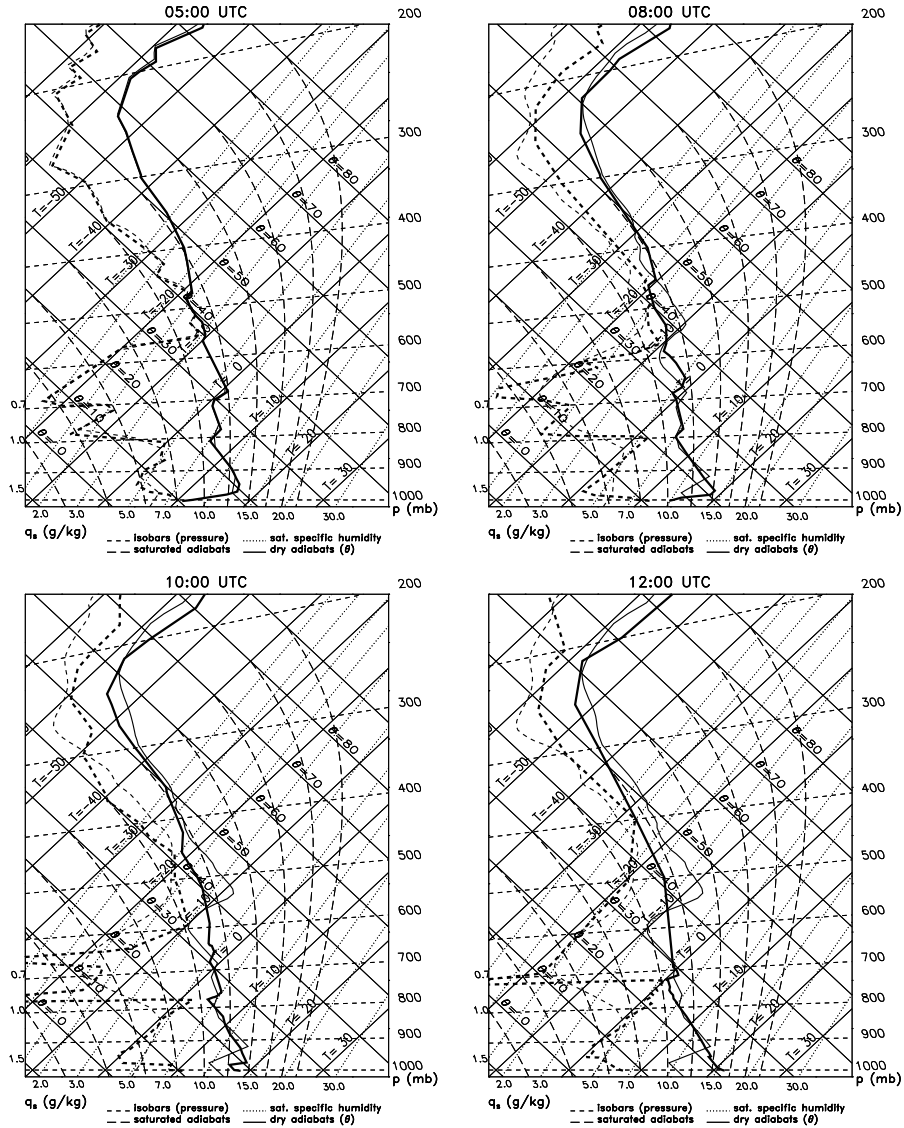


Figure 3. Observed radiosonde profiles (thick lines) from Larkhill on September 5th 2003 from 05:00, 08:00, 10:00 and 12:00 UTC. Note the thin layer at cloud-top that is saturated with respect to liquid water. Modelled profiles, from the forced model run, are shown by the thin lines (these model results are discussed in Section 5(a).)

to apply the method of simulating the Doppler radar data to a 3D study, but unfortunately the computational cost prevented this. Periodic lateral boundary conditions were used, with a rigid lid and no fluxes at the surface. Rayleigh damping was applied above 10 km to remove gravity waves. Spatial resolutions of 100 m in the horizontal and 125 m in the vertical were used, which necessitated an LEM time-step of ≈ 0.8 s.

(a) Initialising the LEM

The four radiosonde profiles, from 05:00, 08:00 10:00 and 12:00 UTC, (Figure 3), were used to initialise the model. Radiosondes sample the near-instantaneous state of the atmosphere at particular points, whilst we wanted to initialise the LEM with mean values. The four windspeed profiles were very similar, but using any individual profile generated an artificially large shear, so the model was initialised with the mean windspeed profile. The shear below 5.5 km produces the slanting fallstreaks observed in Figure 1.

The potential temperature and water vapour profile in the model was initialised with the 05:00 UTC radiosonde profile. Two model runs were then compared. In the first the model was allowed to evolve freely. In the second, in order to account for large scale ascents and descents, the horizontally averaged potential temperature and humidity data in the LEM were relaxed to a value interpolated from the time-series of radiosonde data (using a relaxation timescale of one hour). Using either method, random perturbations of ± 0.1 K and $\pm 5\%$ were added to the initial potential temperature and water vapour mixing ratios fields between 4 and 8 km, to allow cloud inhomogeneities to develop (Starr *et al.*, 2000). In both cases the modelled turbulent kinetic energy increased rapidly for two hours and then more slowly. For this reason the first two hours of the simulations were considered to be model spin-up periods. Further simulations, using surface fluxes from the Met Office Unified model, showed that neglecting surface fluxes had a negligible impact on the cloud for this case. Differences between results from the forced and unforced simulations are discussed in Section 5(a).

(b) Simulating the Doppler radar and backscatter lidar data within the LEM

An LEM profile was extracted every time-step and statistics calculated every thirty seconds in order to simulate the radar data (as done for IWC in Marsham and Dobbie (2005)). Statistics were calculated for the central column of the LEM. These statistics were calculated in the same way as the radar statistics, except that: (1) since at some times the LEM time-step was less than 1.25 s there were between 36 to 40 time-steps in any thirty second interval, rather than the twenty-four intervals used in the radar data. (2) The LEM grid-spacing was 100 m in the horizontal and 125 m in the vertical in the cloudy region, whereas the radar beam is 70 m in the horizontal and 60 m in the vertical at 7 km. The mean IWC[‡] was calculated using all timesteps within the thirty second interval.

The mean Doppler velocity was calculated using all time-steps where there was detectable ice (*i.e.* greater than 2.0×10^{-4} g/m³, the detection limit of the radar) and the standard deviation in Doppler velocity was calculated if at least twenty four time-steps had detectable ice. Overall, it is thought that errors introduced by this difference in the basic time-averaging interval of the data (1.25 s for the radar, $\simeq 0.8$ s for the LEM) and the difference between the spatial resolution of the radar and the LEM are small in this inter-comparison.

To output the Doppler radar statistics from the LEM the fallspeeds routinely calculated for ice and snow in the model had to be converted to a mean mass-squared weighted fallspeed to replicate the Doppler radar data (see the Appendix). In addition to the IWC and Doppler velocities observable by the radar, LEM modelling also allowed statistics of unobservable parameters, such as

[‡] The IWC was output from the LEM, not a radar reflectivity from which IWC could be derived; in this sense the IWC data are not true “simulated data”.

vertical winds and fallspeeds, to be generated with the same averaging in time and space. This then allows us to investigate the relationships between the observable and unobservable parameters for this modelled altocumulus cloud (Section 5(c)), thus the LEM simulation can be used as a test for retrieval algorithms that estimate these “unobservable” parameters from observable ones.

In order to simulate the lidar data the extinction coefficient, α_i , of a hydrometeor species, i , was assumed to be

$$\alpha_i = 1.5 \times \text{WC}_i / (\rho_i r_{ei}), \quad (4)$$

where WC_i is the water content of species i (*i.e.* the LWC or the IWC), ρ_i is the density of liquid water or ice and r_{ei} is the effective radius (Foot, 1988). Effective radius is not a prognostic variable for liquid water in the LEM so a value of $4.18 \mu\text{m}$ was used (as used for the radiative transfer; the minimum value allowed by the parameterisation used). This radius was consistent with radii derived from the LWC using the number concentration of $2.4 \times 10^8 \text{ m}^{-3}$ assumed by the LEM and also *in-situ* observations from other similar mixed-phase clouds (Hogan et al., 2003a). The effective radius for ice and snow were derived from the mass and number concentrations in the LEM. β was estimated using α divided by a “lidar ratio”, or “extinction-to-backscatter ratio”, S ,

$$\beta_i = \alpha_i / S_i. \quad (5)$$

A value of 18.5 sr was assumed for both ice and liquid water. This is an appropriate value for liquid water (Pinnick et al., 1983) and a reasonable mean value for ice, although the value for ice is much more variable, typically 15–50 sr (Grund and Eloranta, 1990), although 5 to 150 has been observed for cirrus (Lynch et al., 2002). The backscatter values were then summed for each hydrometeor species and applied in Equations 2 and 3 to get the attenuated backscatter coefficient, β^l , at each level.

5. RESULTS

We first compare results from the unforced and forced simulations with observed values (Section 5(a)). This shows that profiles from the unforced simulation differ significantly from those observed and in this case the modelled cloud is higher than observed. The unforced model run does not account for large scale ascents or descents and ECMWF 12 to 24 hour forecasts suggest that allowing for these would produce model profiles more similar to those observed. Relaxing the profiles to those observed (to account for these unresolved large scale processes) results in a cloud more similar to the one observed and results from this run are used in the remainder of the paper (Sections 5(b) to (e)).

(a) *The unforced and forced simulations*

Figure 3 shows the observed radiosonde profiles compared with profiles from the freely evolving model run. This shows that by 08:00 UTC the modelled temperature within the cloud-layer was higher than observed (580 hPa to 450 hPa, \simeq 4500 m to 6300 m), due to the latent heat released by condensation and freezing. Similarly, below the cloud the modelled temperature was lower than observed (680 hPa to 580 hPa, \simeq 3200 m to 4500 m), due to sublimation of ice. These deviations from the observed profile grew throughout the simulation until

12 UTC, at an overall rate of approximately 1 K/hour. Vertical winds from 12 to 24 hour ECMWF forecasts suggest a large scale ascent rate of up to 3 cm/s at 8 km and a descent of up to 2 cm/s at 4.5 km. If these ascents were adiabatic they would largely compensate for the observed deviations of the modelled profiles from those observed. Figure 4(a) shows that the unforced model run results in IWC comparable with those observed, but the cloud is higher than observed. Figure 4(b) suggests that turbulence levels were similar to those observed, but larger at cloud-top. This may have led to the cloud-top height increasing too rapidly with time and the cooler than observed cloud-top at 8 UTC (Figure 3).

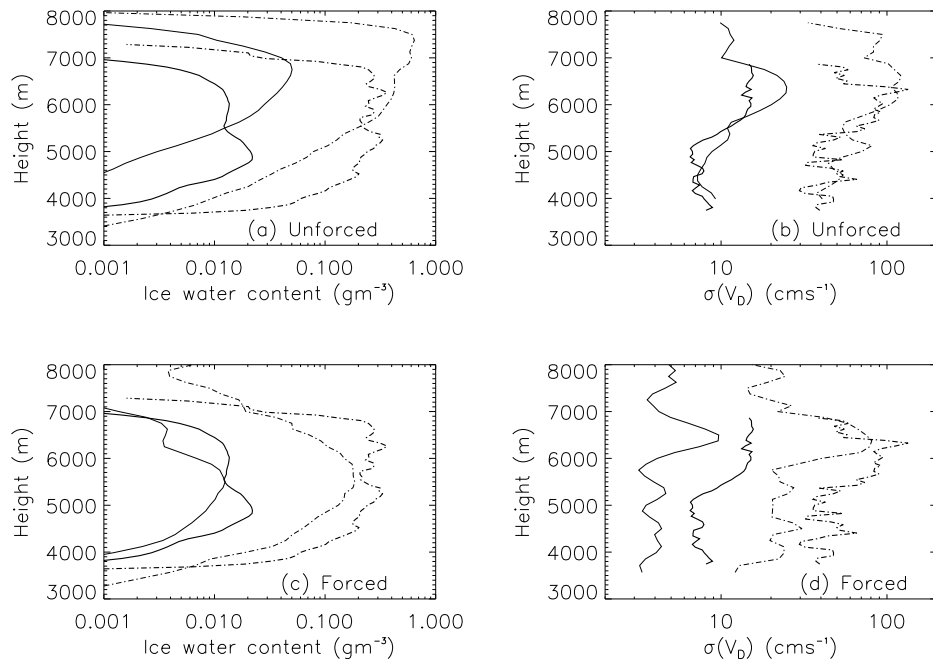


Figure 4. Profiles of: (a) and (c) IWC, (b) and (d) standard deviation in mean Doppler velocity, $\sigma(V_D)$, both between 7 and 12 UTC. Thick and thin lines show observed and modelled values respectively. Mean values are shown by the solid lines and the maximum values by the dash-dot lines. Statistics of $\sigma(V_D)$ were only calculated where this parameter was defined (*i.e.* when a detectable signal was present for all the contributing time-intervals). (a) and (b) are from the unforced simulation, (c) and (d) from the run relaxed to the time-series of observed profiles.

Continuously relaxing the model profile to the observed profiles (Section 4(a)) gave a better agreement with the observed temperature profiles as expected (dew-point and air temperatures within approximately 2 K of those observed). The ECMWF forecasts suggest significant large scale ascents and descents of 2 to 3 cm/s, but without a more complete set of observations, which allow these large scale effects to be more accurately quantified (e.g. Zhang and Lin (2001)), it is not possible to evaluate to what extent the relaxation is accounting for the unresolved large scale processes, and to what extent it is an artificial forcing. However, since we cannot expect the LEM to represent the cloud accurately without accounting

for these large scale processes, the results from the forced model run are used throughout the remainder of the paper.

The run relaxed to the observed profiles captures the observed IWC profile (mean and maximum values) reasonably well, but the observed values at some levels are up to five times the modelled values (Figure 4(b)). This is outside the error bounds on the observations, which are less than a factor of two (Hogan et al., 2006). Overall, the modelled IWP is 0.6 times that observed. The relaxation of the model profile towards those observed has reduced the cloud-top compared with the unforced run and allowed the cloud to deepen more by moistening air below 580 hPa. The relaxation reduces the turbulence in the cloud however, leading to less turbulence than observed (Figure 4(d)).

(b) *Comparing observed and modelled fields*

Figure 5 shows the simulated time-height cross-sections of IWC, standard deviation in Doppler velocity and mean Doppler velocity. More quantitative comparisons of IWC and Doppler velocities are shown in subsequent figures, which show probability density functions (pdfs) of the variables, their inter-dependence and their height dependence. Again considering 05:00 to 07:00 UTC as a spin-up period (Section 5(a)) comparing Figures 1(a) and 5(a) shows that the LEM captures the spatial variability of the IWC remarkably well, although there is more ice above 8 km in the model and too much ice at 7 km before 10 UTC. The orientation and scales of the features are similar in the real and simulated observations. Similarly, comparing Figures 1(b) and 5(b) we see that the model is capturing the increase in the standard deviation in mean Doppler velocity with height (and hence the standard deviation in vertical air-velocity, Section 5(c)), which is caused by the longwave cooling of the cloud-top (also see Figure 4(d)) and also some patchy increases in turbulence near the cloud-base. The values are, however, in general too small. The mean Doppler velocities decrease with height in both the model and the observations (Figures 1(c) and 5(c)), but it should be noted that the simulated mean Doppler velocities are affected by waves in the LEM. The mean vertical wind at any level in the LEM is zero, so time-averaging data from time-height plots of true-air velocities was expected to produce velocities close to zero for long time intervals. This did not occur and this was probably caused by waves propagating in the LEM that had a phase speed similar to the windspeed, but in the opposite direction (the effect was removed if the “radar position” in the LEM was randomly varied at each time-step). Such waves may be artificially maintained by the periodic lateral boundary conditions used in the LEM, but the effect was robust to damping vertical velocities and potential temperatures at the edge of the model domain and varying the strength of the Rayleigh damping layer. The waves were not caused by relaxing to the timeseries of radiosonde data and occurred in unforced model runs (Section 4(a)), or runs using a constant windspeed rather than a sheared profile. However, these waves had a horizontal wavelength of approximately 5 km and so affect the cloud on a timescale of approximately 5 minutes (windspeed \simeq 15 m/s) so are expected to have relatively little effect on the cloud.

The attenuated lidar backscatter from the ice is apparently much larger in the LEM (Figure 6(a)) than in the observations (Figure 2). It is not clear though whether in reality we should be able to observe this modelled backscatter from the ice, since the lowest recorded attenuated backscatters in the observations are a function of the instrument (caused by the proximity of layers giving

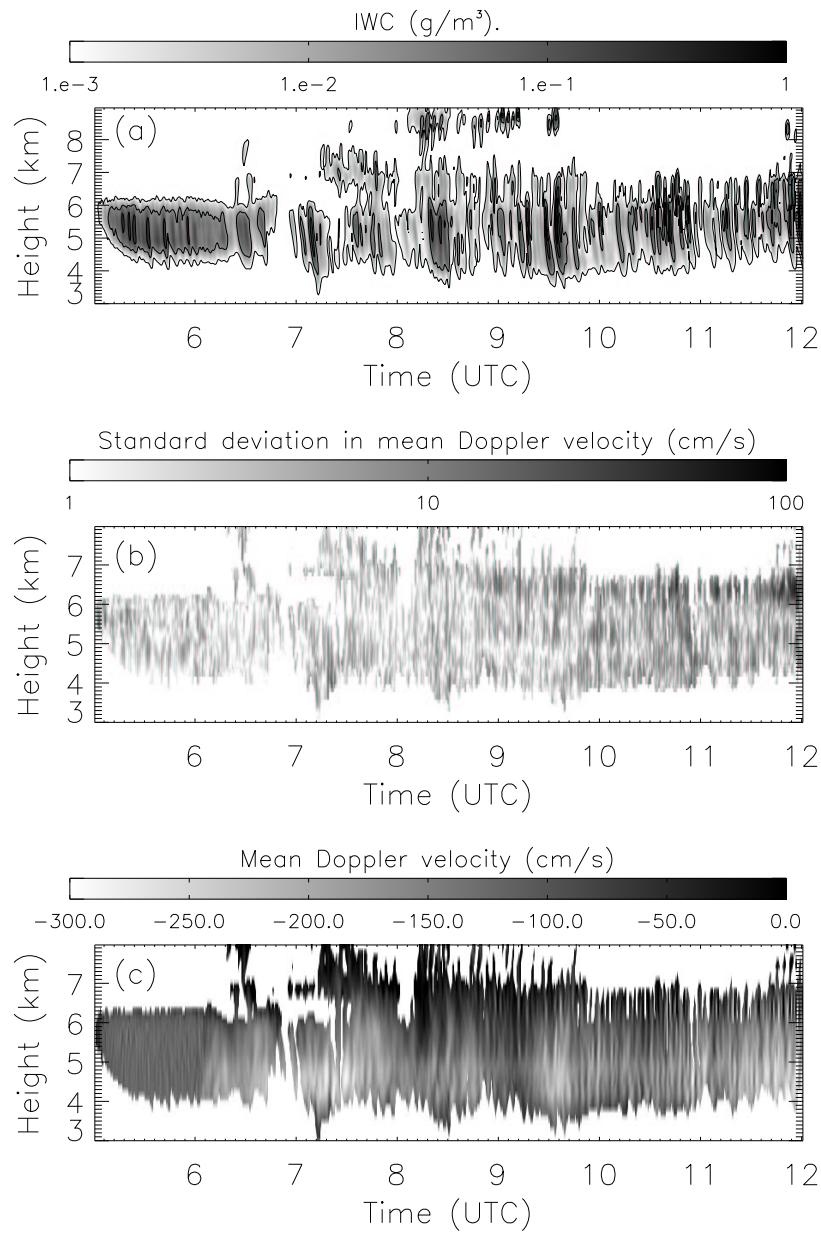


Figure 5. Simulated radar retrievals from the LEM: (a) Ice water content (contours are at 0.001, 0.01, 0.05 and 0.1 g/m^3) (b) The standard deviation in mean Doppler velocity (c) The mean Doppler velocity. The corresponding observations are shown in Figure 1.

significant backscatter) rather than real observations. The daylight also reduces the sensitivity of the instrument. The extinction-to-backscatter ratio, S_{ice} , may also have been under-estimated (a value of 30 sr would halve β'). The LEM produces liquid water cells near cloud-top (≈ 6.8 km) as observed (Figure 2). It clearly captures the cellular nature of the LWC. The base of each liquid cell is

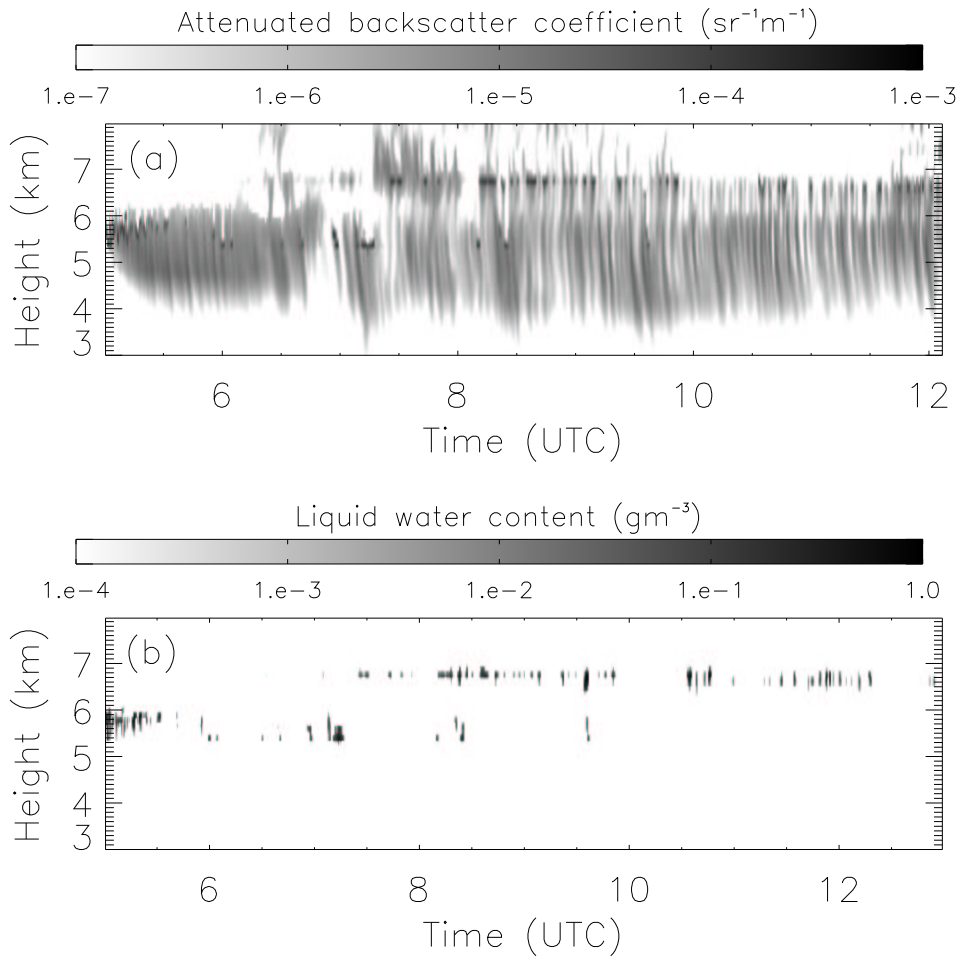


Figure 6. (a) Simulated attenuated lidar backscatter from the LEM (b) the corresponding modelled LWC. Observed lidar data is shown in Figure 2.

detected by the real and simulated lidar, but the beam is rapidly attenuated and in the LEM the liquid water cells are in fact 100 m to 600 m deep (Figure 6(b)). The LEM produces less liquid cloud than observed near cloud base (this was also true for the unforced run, which had turbulence levels more similar to those observed (Figure 4)). Figure 7(a) shows that the LEM tends to over-estimate the mean attenuated backscatter at 5 to 6 km compared with the observations, but as already noted the backscatter from the ice is larger in the LEM than in the observations. The LEM shows peaks in backscatter from the liquid layers and the magnitude of the peaks is comparable with the observed values (Figure 7(b)).

Figure 8 compares the LWP retrieved from the microwave radiometer data and the LEM data. The radiometer beamwidth is 2.3° , giving an instantaneous field-of-view of 200 m by 200 m at a height of 5 km. This is smaller than the size of the liquid water cells in the LEM ($\simeq 1$ km). Figure 8 shows that the maximum LWP observed in a single column of the LEM is approximately half

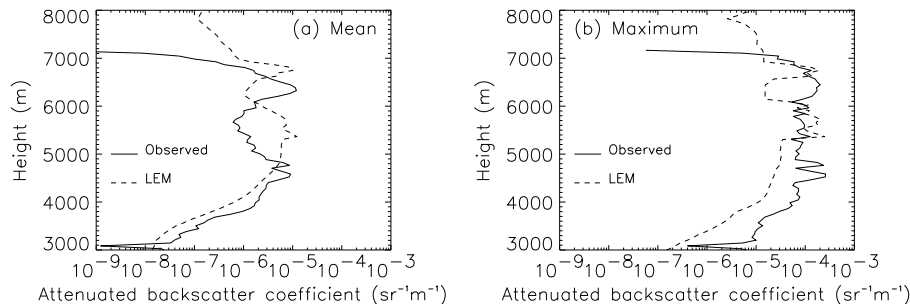


Figure 7. Attenuated lidar backscatter coefficient for the observed (solid line) and simulated (dashed line) data between 7 and 12 UTC. Horizontal means (a) and maxima (b) are shown as a functions of height.

the magnitude of the microwave-radiometer retrievals, whilst the mean LWP in the LEM is 10 to 20% of that observed. This shows that the LEM is producing significantly fewer cells than occurred in reality, which each have a lower LWP than in reality. This hypothesis is supported by photographs from the Chilbolton cloud camera, which showed a continuous liquid water layer with a cellular structure. Persistent supercooled liquid layers in a mixed phase cloud have to be convectively overturning, otherwise the liquid water depleted by glaciation will not be replenished. Therefore, the liquid water content profile within the liquid cells should be close to adiabatic. The LWP of the liquid cells in the LEM are slightly sub-adiabatic and the microwave observations show that there are too few of them. The unforced model run gave larger than observed vertical velocities at cloud-top (Figure 4(b)), but this only increased the LWP to 30% of that observed. Using prognostic ice nuclei (IN) in the LEM would allow ice nucleation, growth and fallout to deplete IN concentrations and so may allow more liquid water to form in the model (as shown by Cotton and Brown (2004) for an idealised altostratus cloud and Rasmussen *et al.* (2002) and Geresdi *et al.* (2005) for freezing drizzle formation). Decreasing the heterogeneous nucleation rate in the LEM (Meyers *et al.*, 1992) by a factor of five did increase the LWP in the model by a factor of approximately 2.3 and decreased the IWP by 15%. This LWP is in better agreement with the observations, which supports this hypothesis. However, with a decreased heterogeneous nucleation rate mean mass-squared-weighted fallspeeds were increased by approximately 4%, presumably since fewer ice particles allowed increased particle growth rates from vapour deposition, which is in poorer agreement with the observations (Section 5(d)). Finally, Figure 9(a) shows that in the LEM most of the liquid-water tends to be in the updraughts, as expected. In addition there is significant coexistence of liquid water and ice in the model. Figure 9(b) shows that ice and liquid water coexist on the 100 m grid-scale of the LEM (as observed by Field *et al.* (2004) in aircraft data), although larger values of IWC tend to be found for lower values of LWC and higher values of LWC tend to occur with lower values of IWC.

Figure 10(a) shows that the probability density functions (pdfs) of IWC in the model and observations are similar, although the probability of any value of IWC greater than 0.03 g/m^3 is up to three times as likely in the radar data and values less than 0.03 g/m^3 are more likely in the model. Comparing the observed

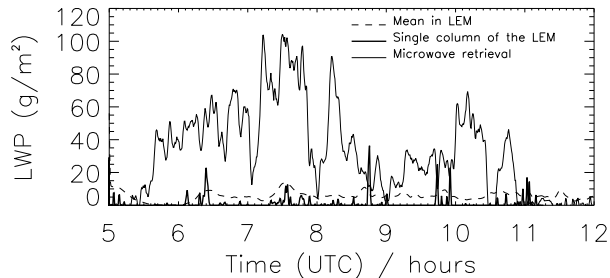


Figure 8. Liquid water paths (LWPs) from the LEM compared with microwave retrievals. “Single column of the LEM” refers to the central column of the model.

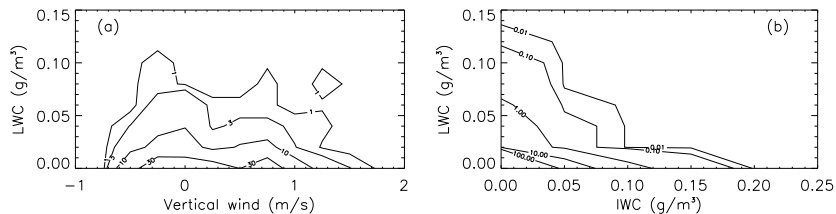


Figure 9. Bivariate probability density functions of (a) liquid water content and vertical winds (for LWCs greater than $2.0 \times 10^{-3} \text{ g/m}^3$) and (b) ice water content and liquid water content (where either the LWC or the IWC is greater than $2.0 \times 10^{-3} \text{ g/m}^3$) from the LEM data between 7 and 12 UTC.

and modelled pdfs of standard deviation in mean Doppler velocity (Figure 10(b)) shows that the LEM gives far fewer values between 7 cm/s and 50 cm/s. Figure 11 shows that the relationship between IWC and $\sigma(V_D)$ is similar in the model and observations, with large standard deviations in Doppler velocities tending to occur with low IWC; these occur at the edge of the convective cells in the LEM. The relative magnitudes of the distributions differ, however, since there are differences between the modelled and observed pdfs of IWC and $\sigma(V_D)$ (as noted for Figure 10).

(c) *The modelled relationship between standard deviations in Doppler velocities and air velocities*

An advantage of simulated radar data is that the modelled standard deviation in Doppler velocity, $\sigma(V_D)$, can easily be compared with the modelled standard deviation in air velocity, $\sigma(w)$. This allows the hypothesis that $\sigma(w)$ dominates $\sigma(V_D)$ in ice clouds (Bouniol et al., 2003) to be tested. Figure 12(a) shows that this is true in this mixed-phase cloud, particularly for the standard deviations greater than 12 cm/s. For values of $\sigma(V_D)$ less than 12 cm/s, $\sigma(V_D)$ tends to provide an overestimate of $\sigma(w)$. This occurs because the variance in V_Z becomes comparable with the variance in w for small values of w (Figure 12(b)). This contribution of $\sigma(V_Z)$ to $\sigma(V_D)$ is larger than that observed by Lothon et al. (2005) for marine stratocumulus, since the fallspeeds of ice and snow are more

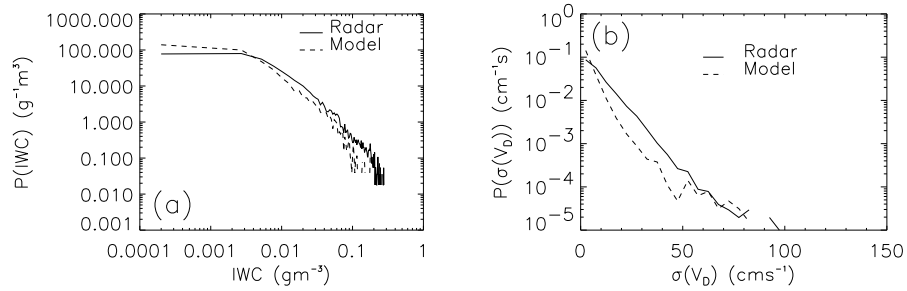


Figure 10. Probability density functions (pdfs) of (a) ice water content (IWC), and (b) standard deviation in mean Doppler velocities ($\sigma(V_D)$) between 7 and 12 UTC. Statistics are only calculated between heights of 3000 m to 8000 m and where: (a) IWC are greater than $2.0 \times 10^{-4} \text{ g/m}^3$ (b) $\sigma(V_D)$ are greater than 1 cm/s.

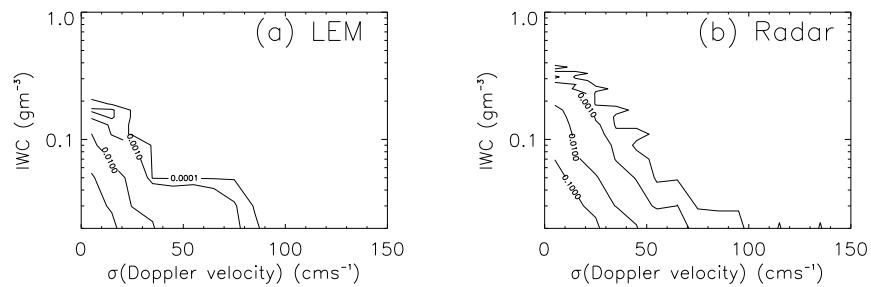


Figure 11. Bivariate probability density functions (pdfs) of ice water content IWC and standard deviation in mean Doppler velocities, $\sigma(V_D)$, from (a) the LEM data and (b) the radar between 7 and 12 UTC. Statistics have been calculated for data between heights of 3000 m and 8000 m and where the IWC is greater than $2.0 \times 10^{-4} \text{ g/m}^3$ and $\sigma(V_D)$ is greater than 1 cm/s.

comparable with the vertical air velocities than the fallspeeds of liquid cloud droplets.

We expect the standard deviation in Doppler velocities to depend on not only the magnitudes of the vertical air velocities, but also on the structure of the embedded convection. So, even though the standard deviations in Doppler velocities are dominated by the standard deviations in air velocities, it is difficult to compare modelled spatial fields of vertical velocities and observed time-height cross sections of standard deviations in Doppler velocities, without simulating the spatial and temporal sampling of the radar within the LEM (as we have done).

The success of this approach in evaluating the relationship between $\sigma(w)$ and $\sigma(V_Z)$ suggest that it may be worth following a similar approach to investigate observed Doppler spectral widths. The sub-grid vertical velocities and sub-grid variance in fallspeeds in the LEM (from the assumed gamma distribution of particle sizes) could be combined to give a simulated Doppler spectral width. This may allow the relative contributions of the variations in vertical velocities and fallspeeds to Doppler spectral width to be evaluated.

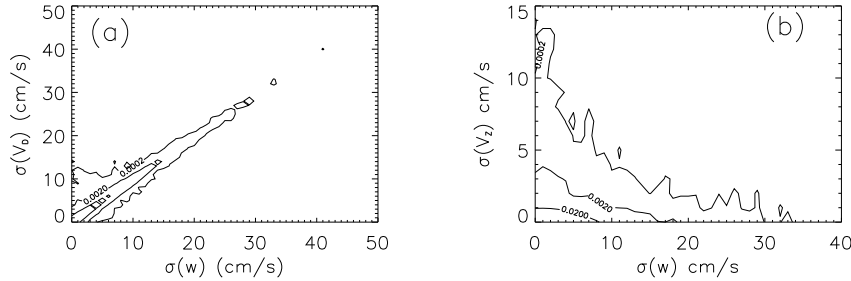


Figure 12. Bivariate pdfs of: (a) simulated standard deviations in Doppler velocities and vertical air velocities ($\sigma(V_D)$ and $\sigma(w)$) (b) simulated standard deviations in vertical air velocities and mass-squared-weighted fallspeeds ($\sigma(w)$ and $\sigma(V_Z)$). Data from between 7 and 12 UTC were used and contours are at $2. \times 10^{-4}$, $2. \times 10^{-3}$ and $2. \times 10^{-2}$ in both plots.

(d) *Time-smoothing Doppler velocities to retrieve fallspeeds*

Time-averaged observed Doppler velocities and time-averaged mass-squared-weighted fallspeeds from the LEM were compared to evaluate the fallspeeds in the LEM. Time-averaging Doppler radar velocities is intended to remove the time-varying contribution of the vertical winds, allowing retrieval of mass-squared-weighted fallspeeds (e.g. Matrosov et al. (1994), or Matrosov and Heymsfield (2000)). However, the simulated radar data did not allow the accuracy of the time-averaging method to be evaluated for this cloud, since, as noted in Section 5(b), time-smoothing the modelled vertical winds showed that these did not average to zero, because of waves in the LEM. Time-averaging the radar observations also relies on the radar pointing absolutely vertically upwards. The accuracy of this is better than $\pm 0.5^\circ$ for the Chilbolton 94 GHz radar, but even an error of 0.2° will result in an error of 5 cm/s for a windspeed of 15 m/s (so this technique is best suited to less windy conditions).

Figure 13 shows that fallspeeds are larger in the LEM than in the observations. The difference is approximately 40 cm/s below 8 km. This is larger than the errors expected from any deviation of the radar from the vertical ($\simeq 5$ cm/s) or any large scale uplift ($\simeq 3$ cm/s). It is not clear why the LEM is giving larger fallspeeds than observed, especially since the modelled IWC is lower than observed (Figure 4(c)). Without observations of particle size we do not know if the LEM is over-estimating the particle sizes, or whether it is over-estimating the terminal fallspeeds of ice particles of the correct size (or both). Reducing the fallspeeds in the LEM by a factor of two thirds and rerunning the model gave a fallspeed profile in better agreement with the observations (Figure 14(b)). This did not significantly change the mean LWP compared to the standard run (the mean LWP was increased by 4%) and gave larger IWC, up to twice those observed (Figure 14(a)).

Figure 15 shows the time-smoothed data from half hour intervals, for which there was data for all the thirty second intervals used in the time-smoothing. The modelled distribution is too bimodal, due to the distinct classes of ice and snow in the LEM. The fallspeeds are not well correlated with the IWC in either the observations or the model and there is a wide spread of fallspeeds for any IWC. This result suggests that although a parameterisation of fallspeeds based on IWC

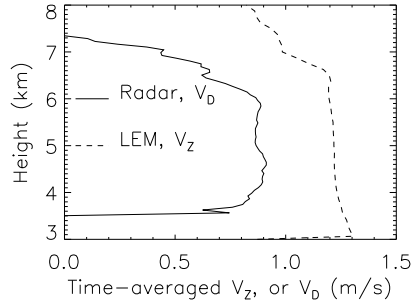


Figure 13. Time averaged mass-squared-weighted terminal fallspeeds, V_Z , from the LEM (dashed line) compared with time-averaged Doppler velocities, V_D , from the radar (solid line). 7 to 12 UTC.

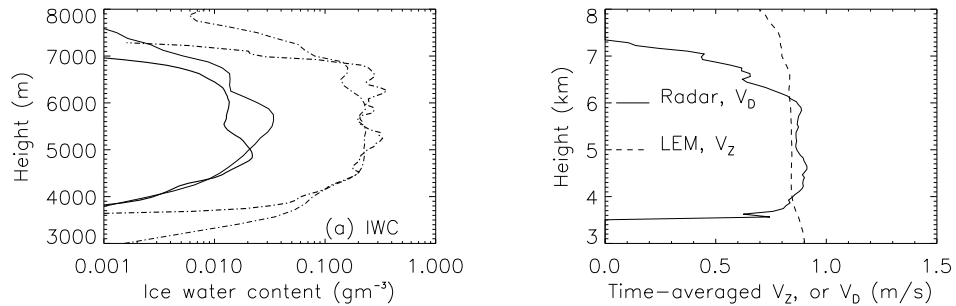


Figure 14. Data from a run with reduced fallspeeds (two thirds their standard values) (a) as Figure 4(c) and (b) as Figure 13.

(for example Matrosov and Heymsfield (2000) for ice clouds) maybe better than using a fixed value, it is by no means ideal (since large numbers of small crystals can give large IWCs with low fallspeeds and a small number of large crystals can give the same IWC, with much larger fallspeeds).

(e) *Contribution of liquid water to the modelled radiative processes*

We expect the liquid water at cloud-top to enhance longwave cooling and reflect a significant fraction of the incoming solar radiation to space (since the small liquid water droplets reflect the shortwave radiation more effectively than the larger ice-crystals). Figure 16 shows the effects of removing the interaction between the LWC and the radiation scheme in the LEM in order to investigate to what extent these processes feedback on to the cloud structure. The LWC increases the cloud-top radiative cooling rate by up to 50% (at 7.2 km, Figure 16(a)). It also increases the total reflected solar radiation at the top of the modelled atmosphere by up to 30 W/m², or 8% (not shown). These processes have raised the height of the maximum LWC by ≈ 200 m at 10 UTC (Figure 16(b)), since the LWC tends to form in the strong updraughts in the LEM, which occur at cloud top and are driven in part by the radiative processes.

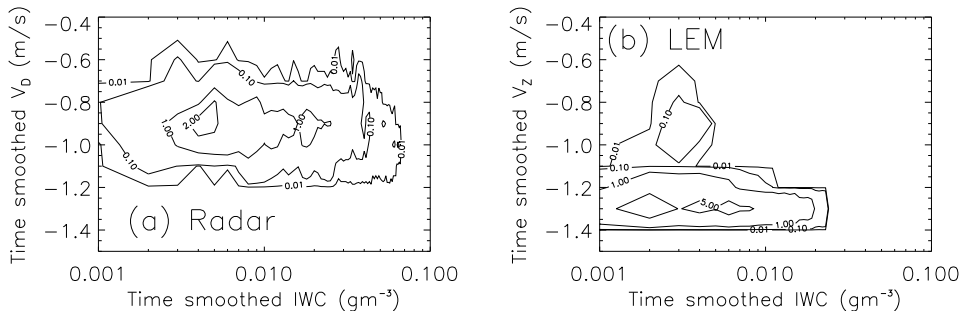


Figure 15. Bivariate pdfs of time averaged IWC and (a) Doppler velocities from the radar (b) fallspeeds from the LEM. Time-averaging was performed over thirty minute intervals for heights between 3 km and 8 km.

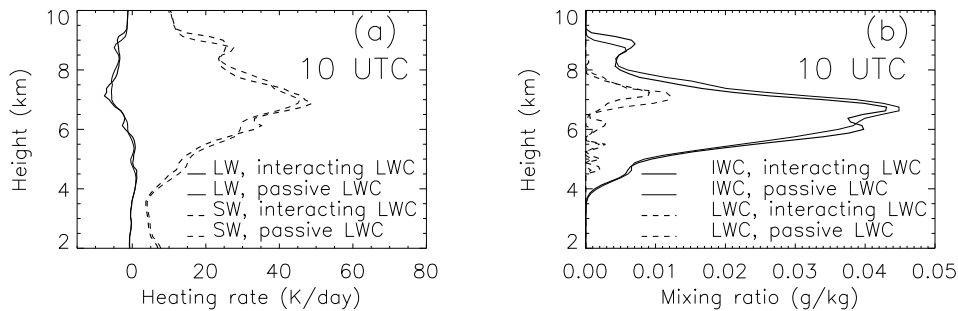


Figure 16. Modelled profiles of (a) radiative heating rates (b) mixing ratios, both at 10 UTC. “Passive LWC” indicates profiles where the interaction between the LWC and the longwave and shortwave radiation has been switched off in the model. “Interacting LWC” indicates where both the IWC and the LWC have been allowed to interact with the radiation.

6. CONCLUSIONS

We have simulated a case of mixed-phase altocumulus observed by the Chilbolton 94 GHz cloud radar, 905 nm lidar and a dual wavelength microwave radiometer. Simulating the Doppler radar and lidar observations within the LEM has allowed us to account for the temporal and spatial sampling of the observing instruments and so compare modelled and observed quantities. In addition, this has allowed us to explore relationships between observed quantities and modelled quantities, (e.g. the standard deviation in mean Doppler velocity and vertical winds). The observations have allowed us to compare modelled and observed IWC, LWP, turbulence, fallspeeds and the locations of LWC, but not ice particle sizes or number concentrations. The evaluation of the LEM is limited by the model initialisation and forcing used (*i.e.* a relaxation to a time-series of radiosondes to account for unresolved large-scale forcings), since accurate large-scale advective tendencies are not available for the Chilbolton radar site. We have however provided a framework for comparison between observations and models that could

be applied to sites with more complete observations, such as the Atmospheric Radiation Measurement (ARM) program sites. In addition, there are very few comparisons between models and observations of mixed-phase layer clouds in the literature and the simulations highlight cloud processes that must be represented if mixed-phase clouds are to be well modelled by GCMs.

The LEM produced a cloud that was realistic in a number of respects: (1) the profile, pdf and time-height field of IWC were similar to those observed (the modelled IWP was approximately 60% of that observed), (2) the LEM produced a layer of supercooled water at cloud top, (3) the standard deviations in vertical winds were 1.5 to 4 times smaller than observed (although values for the unforced model run were similar to observed). A comparison with the LWP retrieved from a dual-wavelength microwave radiometer showed that the LWPs of the liquid cells at cloud-top in the LEM were too small (up to 50% of that observed), and that there were too far few liquid cells. This was also the case in the unforced model run, which had greater than observed turbulence at cloud-top. It is possible that using prognostic ice nuclei in the LEM would allow depletion of ice nuclei by nucleation and so allow more liquid water to form in the model. This hypothesis is supported by the fact that when the heterogeneous ice nucleation rate was decreased by a factor of five in the LEM the modelled LWP was increased by a factor of 2.3, and the IWP decreased by 15%.

Comparing time-smoothed observed mean Doppler velocities and time-smoothed simulated mass-squared-weighted fallspeeds showed that observed fallspeeds were approximately two thirds of modelled values. Reducing the fallspeeds in the LEM, so that they agreed with the observations, gave similar LWC profiles to the standard run, but increased the IWC, giving an IWP 1.6 times that observed. Without observations of mean particle size, or ice number concentration, it is not clear whether the fallspeeds in the LEM are larger than observed from over-estimating the fallspeeds for particles of the correct size, or over-estimating the sizes of the particles. There was little observed or modelled dependence of fallspeeds on IWC, highlighting the limitations of basing fallspeed parametrisations on only the IWC.

Simulating Doppler radar data within the LEM showed that for standard deviations in Doppler velocities, $\sigma(V_D)$, greater than $\simeq 12$ cm/s the modelled standard deviation in Doppler velocities provided an almost unbiased estimate of the modelled standard deviation in vertical winds, $\sigma(w)$. For smaller values of $\sigma(V_D)$, $\sigma(V_D)$ tended to be an over-estimate of $\sigma(w)$. Modelling Doppler spectral widths would allow a better understanding of the relative contributions of variations in vertical winds and fallspeeds to this observed parameter.

In the LEM the thin layer of liquid water at cloud-top contributed significantly to the radiative cooling at the cloud top and the shortwave reflectivity. This fed back onto the cloud dynamics to a limited extent, raising the height of the maximum LWC by 200 m.

Many numerical weather prediction (NWP) models failed to give a good forecast for this case. The results show the importance of using separate prognostic ice and liquid water in NWP models, using a vertical resolution that captures the thin layers of liquid water and accurately representing the sub-grid vertical velocities that allow liquid water to form. The results also show the potential significance of the local depletion of ice-nuclei within mixed-phase clouds and so using prognostic ice nuclei in the LEM. The success of the LEM in representing

this case demonstrates its potential as a tool for the development of parametrisations for future NWP and climate models.

ACKNOWLEDGEMENTS

The authors would like to acknowledge the Cloudnet project (EU project EUK2-2000-00611) for radar, lidar and radiometer data from the Chilbolton Facility for Atmospheric and Radio Research (part of the Rutherford Appleton Laboratory) and the NWP model output. Nicolas Gaussiat performed the microwave radiometer retrieval. Radiosonde data were obtained from the Met Office. In addition the authors would like to thank the helpful comments of the two anonymous referees. This work was funded by the Natural Environment Research Council (NERC: NER/M/S/2002/00127).

APPENDIX

Calculation of mass-squared-weighted fallspeeds in the LEM

As described by Gray et al. (2001), the LEM assumes a relationship between diameter, D , and fallspeed, $V(D)$, for each hydrometeor species, x (*i.e.* ice or snow in this case),

$$V_x(D) = a_x D^{b_x} \left(\frac{\rho_0}{\rho} \right)^{0.5}, \quad (\text{A.1})$$

where a_x , b_x are constants, which depend on the hydrometeor type (Gray et al., 2001; Lin et al., 1983; Ferrier et al., 1994), ρ is the air density and ρ_0 the surface air density. The mass, $M_x(D)$, of a particle of diameter D is

$$M_x(D) = c_x D^{d_x}, \quad (\text{A.2})$$

where c_x and d_x are again constants for each hydrometeor species (Swann, 1998; Gray et al., 2001). A gamma distribution is assumed for the size distribution, $n_x(D)$,

$$n_x(D) = n_{x0} D^{\alpha_x} \exp[-\lambda_x D], \quad (\text{A.3})$$

where α_x is the shape parameter (Gray et al., 2001; Swann, 1998). The double moment scheme in the LEM (used for ice and snow in this paper) has prognostic equations for both the total number concentration, N_x , and the total mass mixing ratio, q_x . Given these variables it can be shown that the parameters for the size distribution, n_{x0} (the intercept parameter) and λ_x (the slope parameter) are given by,

$$n_{x0} = \frac{\rho N_x \lambda_x^{(1+\alpha_x)}}{\Gamma(1+\alpha_x)}, \quad (\text{A.4})$$

and

$$\lambda_x = \left(\frac{N_x c_x \Gamma(1+\alpha_x + d_x)}{M_x \Gamma(1+\alpha_x)} \right)^{\frac{1}{d_x}}. \quad (\text{A.5})$$

The mean mass-weighted fallspeed, V_{M_x} , is then,

$$V_{M_x} = a_x \left(\frac{\rho_0}{\rho} \right)^{0.5} \frac{\Gamma(d_x + \alpha_x + b_x + 1)}{\Gamma(1 + \alpha_x + d_x)} \lambda^{-b_x}, \quad (\text{A.6})$$

(Gray *et al.*, 2001). Furthermore, it can be shown that this gives a mass-squared weighted fallspeed, V_{Z_i} , of

$$V_{Z_i} = a_i \left(\frac{\rho_0}{\rho} \right)^{0.5} \frac{\Gamma(2d_i + \alpha_i + b_i + 1)}{\Gamma(1 + \alpha_i + 2d_i)} \lambda^{-b_i}, \quad (\text{A.7})$$

for a single species, i , with a weighted average required when both ice and snow are present.

REFERENCES

- Bouniol, D., Illingworth, A. J., and Hogan, R. J. 2003 ‘Deriving turbulent kinetic energy dissipation rate within clouds using ground based 94 GHz radar’, Proc. 31st AMS Conf. on Radar Meteorology, Seattle.
- Clark, P. D., Choullarton, T. W., Brown, P. R. A., Field, P. R., Illingworth, A. J., and Hogan, R. J. 2005 Numerical modelling of mixed-phase frontal clouds observed during the CWVC project, *Quart. J. Roy. Meteor. Soc.*, **131**, 1677–1694.
- Cotton, R. J. and Brown, P. R. A. 2004 ‘Ice initiation and evolution in large-eddy simulations using prognostic ice nuclei and CCN’, 11th Conference on Cloud Physics, **P2**.
- Dobbie, S. and Jonas, P. 2001 Radiative influences on the structure and lifetime of cirrus clouds, *Quart. J. Roy. Meteor. Soc.*, **127**, 2663–2682.
- Ferrier, B. S., Tao, W. K., and Simpson, J. 1994 A double moment multiple phase four class bulk ice scheme. Part II: Simulations of convective storms in different large scale environments and comparisons with other bulk parametrizations, *J. Atmos. Sci.*, **51**, 249–280.
- Field, P. R., Hogan, R. J., Brown, P. R. A., Illingworth, A. J., Choullarton, T. W., Kaye, P. H., Hirst, E., and Greenaway, R. 2004 Simultaneous radar and aircraft observations of mixed-phase cloud at the 100-m-scale, *Quart. J. Roy. Meteor. Soc.*, **130**, 1877–1904.
- Fleishauer, R. P., Larson, V. E., and Vonder Haar, T. H. 2002 Observed microphysical structure of midlevel, mixed-phase clouds, *J. Atmos. Sci.*, **59**, 1779–1804.
- Foot, J. S. 1988 Some observations of the optical-properties of clouds. 2. Cirrus, *Quart. J. Roy. Meteor. Soc.*, **114**, 145–164.
- Fu, Q. 1996 An accurate parameterization of the solar radiative properties of cirrus clouds for climate models, *J. Climate*, **9**, 2058–2082.
- Fu, Q. and Liou, K. N. 1992 On the correlated k -distribution method for radiative transfer in nonhomogeneous atmospheres, *J. Atmos. Sci.*, **49**, 2139–2156.
- Fu, Q. and Liou, K. N. 1993 Parameterization of the radiative properties of cirrus clouds, *J. Atmos. Sci.*, **50**, 2008–2025.
- Fu, Q., Yang, P., and Sun, W. B. 1998 An accurate parameterization of the infrared radiative properties of cirrus clouds for climate models, *J. Climate*, **11**, 2223–2237.
- Geresdi, I., Rasmussen, R., Grabowski, W. and Bernstein, B. 2005 Sensitivity of freezing drizzle formation in stably stratified clouds to ice processes, *Meteorol. Atmos. Phys.*, **88**, 91–105.

- Gray, M. E. B., Petch, J., Derbyshire, S. H., Brown, A. R., Lock, A. P., and Swann, H. A. 2001 'Version 2.3 of the Met. Office large eddy model', The Met. Office, Exeter, UK.
- Grund, C. J. and Eloranta, E. W. 1990 The 27-28 OCTOBER 1986 FIRE IFO cirrus case-study - cloud optical-properties determined by high spectral resolution lidar, *Mon. Weather Rev.*, **118**, 2344–2355.
- Heymsfield, A. J. and Iaquinta, J. 2000 Cirrus crystal terminal velocities, *J. Atmos. Sci.*, **57**, 916–938.
- Heymsfield, A. J., Milosevich, L. M., and Slingo, A. 1991 An observational and theoretical study of highly supercooled altocumulus, *J. Atmos. Sci.*, **48**, 923–945.
- Hogan, R. J., Francis, P. N., Flentje, H., Illingworth, A. J., Quante, M., and Pelon, J. 2003a Characteristics of mixed-phase clouds: Part I: Lidar, radar and aircraft observations from CLARE'98, *Quart. J. Roy. Meteor. Soc.*, **129**, 2089–2116.
- Hogan, R. J., Illingworth, A. J., O'Connor, E. J., and Poiares Baptista, J. P. V. 2003b Characteristics of mixed-phase clouds: Part II: A climatology from ground-based lidar, *Quart. J. Roy. Meteor. Soc.*, **129**, 2117–2134.
- Hogan, R. J., Behera, M. D., O'Connor, E. J., and Illingworth, I. J. 2004 Estimating the global distribution of supercooled liquid water clouds using the LITE lidar, *Geophys. Res. Lett.*, **31**, L05106, doi:10. 1029/2003GL018977.
- Hogan, R. J., Mittermaier, M. P., and Illingworth, A. J. 2005 'The retrieval of ice water content from radar reflectivity factor and temperature and its use in the evaluation of a mesoscale model', Accepted *J. Appl. Meteorol.*
- Korolev, A. and Isaac, G. 2003 Roundness and aspect ratio of particles in ice clouds, *J. Atmos. Sci.*, **60**, 1795–1808.
- Li, Z. X. and Le Treut, H. 1992 Cloud-radiation feedbacks in a general circulation model and their dependence on cloud modelling assumptions, *Clim. Dyn.*, **7**, 133–139.
- Lin, Y. L., Farley, R. D., and Orville, H. 1983 Bulk parametrization of the snow field in a cloud model, *J. Climate Appl. Met.*, **22**, 1065–1092.
- Liu, S. and Krueger, S. K. 1995 'Numerical simulations of altocumulus with a cloud resolving model', Proceedings of the 5th Atmospheric Radiation Measurement ARM Science team meeting, DOE CONF-9503140, San Diego, California.
- Liu, S. and Krueger, S. K. 1998 Numerical simulations of altocumulus using a cloud resolving model and a mixed layer model, *Atm. Res.*, **47-48**, 461–474.
- Lothon, M., Lenschow, D. H., Leon, D. and Vali, G. 2005 Turbulence measurements in marine stratocumulus with airborne Doppler radar, *Q. J. Roy. Met. Soc.*, **131**, 2063–2080.
- Lynch, D. K., Sassen, K., Starr, D. O'C. and Stephens, G. (Editors) 2002 *Cirrus*, Oxford University Press, New York
- Marsham, J. and Dobbie, S. 2005 The effects of wind shear on cirrus: an LEM and radar case study, accepted by *Quart. J. Roy. Meteor. Soc.*
- Matrosov, S. Y. and Heymsfield, A. J. 2000 Use of Doppler radar to assess ice cloud particle fall velocity-size relations for remote sensing and climate studies, *J. of Geophys. Res.*, **105**, 22427–22436.

- Matrosov, S. Y., Orr, B. W., Kropfli, R. A., and Snider, J. B. 1994 Retrieval of vertical profiles of cirrus cloud microphysical parameters from Doppler radar and infrared radiometer measurements, *J. Appl. Meteorol.*, **33**, 617–626.
- Matveev, L. T. 1984 *Cloud dynamics*. D. Reidel Pub. Co.
- Meyers, M. P., DeMott, P. J., and Cotton, W. R. 1992 New primary ice nucleation parameterizations in an explicit cloud model, *J. Appl. Meteorol.*, **31**, 708–721.
- Pinnick, R. G., Jennings, S. G., Chylek, P., Ham, C., and Grandy, W. T. 1983 Backscatter and extinction in water clouds, *J. of Geophys. Res.*, **88**, 6787–6796.
- Rasmussen, R. M., Geresdi, I., Thompson, G., Manning, K. and Karplus, E. 2002 Freezing drizzle formation in stably stratified layer clouds: The role of radiative cooling of cloud droplets, cloud condensation nuclei, and ice initiation, *J. Atmos. Sci.*, **59**, 837–860.
- Rauber, R. M., Tokay, A. 1991 An explanation for the existence of supercooled water at the top of cold clouds, *J. Atmos. Sci.*, **48**, 1005–1023.
- Starr, D. O., Benedetti, A., Boehm, M., Brown, P. A., Gierens, K. M., Girard, E., Giraud, V., Jakob, C., Jensen, E. A., Khvorostyanov, V., Koehler, M., Lare, A., Li, R., Maruyama, K., Montero, M., Tao, W., Wang, Y., and Wilson, D. 2000 ‘Comparison of cirrus cloud models: A project of the GEWEX cloud systems study (GCSS) working group on cirrus cloud systems’, 13th International conference on clouds and precipitation, Reno, **1**, 1–4.
- Starr, D. O. and Cox, S. K. 1985 Cirrus clouds. Part I: Numerical experiments on the formation and maintenance of cirrus, *J. Atmos. Sci.*, **42**, 2682–2694.
- Stephens, G. L., Vane, D. G., Boain, R. J., Mace, G. G., Sassen, K., Wang, Z. E., Illingworth, A. J., O’Connor, E. J., Rossow, W. B., Durden, S. L., Miller, S. D., Austin, R. T., Benedetti, A., and Mitrescu, C. 2002 The Cloudsat mission and the A-train - a new dimension of space-based observations of clouds and precipitation, *Bull. Am. Met. Soc.*, **83**, 1771–1790.
- Sun, Z. and Shine, K. P. 1995 Parameterization of ice cloud radiative properties and its application to the potential climatic importance of mixed-phase clouds, *J. Clim.*, **8**, 1874–1888.
- Swann, H. 1998 Sensitivity to the representation of precipitating ice in CRM simulations of deep convection, *Atm. Res.*, **48**, 415–435.
- Tremblay, A. and Glazer, A. 2000 An improved modeling scheme for freezing precipitation forecasts, *Mon. Weather Rev.*, **128**, 1289–1308.
- Tremblay, A., Vaillancourt, P. A., Cober, S. G., Glazer, A. and Isacc, G. A. 2003 Improvements of a Mixed-Phase Cloud Scheme Using Aircraft Observations, *Mon. Weather Rev.*, **131**, 672–686.
- Vaillancourt, P. A., Tremblay, A., Cober, S. G. and Isacc, G. A. 2003 Comparison of aircraft observations with mixed-phase cloud simulations, *Mon. Weather Rev.*, **131**, 656–671.

- Warren, S. G., Hahn, J., London, R. M., Chervin, R. M., and Jenne, R. 1986 ‘Global distribution of total cloud cover and cloud type over land’, NCAR Tech. Note, TN-273 (STR, 229).
- Warren, S. G., Hahn, J., London, R. M., Chervin, R. M., and Jenne, R. 1988 ‘Global distribution of total cloud cover and cloud type over the ocean’, NCAR Tech. Note, TN-317 (STR, 212).
- Westwater, E. R. 1978 Accuracy of water-vapour and cloud liquid determination by dual-frequency ground-based microwave radiometry, *Radio Science*, **13**, 677–685.
- Wilson, D. R. and Ballard, S. P. 1999 A microphysically based precipitation scheme for the UK Meteorological Office unified model, *Quart. J. Roy. Meteor. Soc.*, **125**, 1607–1636.
- Xu, K. M., Cederwall, R. T., Donner, L. J., Grabowski, W. W., Guichard, F., Johnson, D. E., Khairoutdinov, M., Krueger, S. K., Petch, J. C., Randall, D. A., Seman, C. J., Tao, W. K., Wang, D. H., Xie, S. C., Yio, J. J., and Zhang, M. H. 2002 An intercomparison of cloud-resolving models with the atmospheric radiation measurement summer 1997 intensive observation period data, *Quart. J. Roy. Meteor. Soc.*, **128**, 593–624.
- Zhang, M. H. and Lin, J. L. 2001 Objective analysis of ARM IOP data: method and sensitivity, *Mon. Weather Rev.*, **129**, 295–311.